LETTER

https://doi.org/10.1038/s41586-018-0450-2

Synthetic three-dimensional atomic structures assembled atom by atom

Daniel Barredo[1,2]*, Vincent Lienhard[1,2], Sylvain de Léséleuc[1,2], Thierry Lahaye[1] & Antoine Browaeys[1]

A great challenge in current quantum science and technology research is to realize artificial systems of a large number of individually controlled quantum bits for applications in quantum computing and quantum simulation. Many experimental platforms are being explored, including solid-state systems, such as superconducting circuits[1] or quantum dots[2], and atomic, molecular and optical systems, such as photons, trapped ions or neutral atoms[3–7]. The latter offer inherently identical qubits that are well decoupled from the environment and could provide synthetic structures scalable to hundreds of qubits or more[8]. Quantum-gas microscopes[9] allow the realization of two-dimensional regular lattices of hundreds of atoms, and large, fully loaded arrays of about 50 microtraps (or 'optical tweezers') with individual control are already available in one[10] and two[11] dimensions. Ultimately, however, accessing the third dimension while keeping single-atom control will be required, both for scaling to large numbers and for extending the range of models amenable to quantum simulation. Here we report the assembly of defect-free, arbitrarily shaped three-dimensional arrays, containing up to 72 single atoms. We use holographic methods and fast, programmable moving tweezers to arrange—atom by atom and plane by plane—initially disordered arrays into target structures of almost any geometry. These results present the prospect of quantum simulation with tens of qubits arbitrarily arranged in space and show that realizing systems of hundreds of individually controlled qubits is within reach using current technology.

Three-dimensional atomic arrays at half filling have been obtained using optical lattices with large spacings[12], which facilitate single-site addressability and atom manipulation[13]. As an alternative approach, here we use programmable holographic optical tweezers to create three-dimensional (3D) arrays of traps. Holographic methods offer the advantage of higher tunability of the lattice geometry because the design of optical potential landscapes is reconfigurable and only limited by diffraction[14–16]. In our experiment[14], arbitrarily designed arrays of up to about 120 traps are generated by imprinting a phase pattern on a dipole trap beam at 850 nm with a spatial light modulator (Fig. 1a). This phase mask is calculated using the 3D Gerchberg–Saxton algorithm, simplified for the case of point traps[17]. The beam is then focused with a high-numerical-aperture (0.5) aspheric lens under vacuum, creating individual optical tweezers with a measured $1/e^2$ radius of about 1.1 μm and a Rayleigh length of approximately 5 μm. After recollimation with a second aspheric lens, the intensity of the trapping light is measured using a standard charge-coupled device (CCD) camera. An electrically tunable lens (ETL1) in the imaging path allows us to acquire series of stack images along the optical axis z, from which we reconstruct the full 3D intensity distribution. The imaging system covers a z-direction scan range of 200 μm.

Figure 1b–d shows some examples of patterns suitable for experiments with single atoms. The images are reconstructed using a maximum-intensity projection method[18] from 200 z images obtained with the diagnostics CCD camera. With about 3.5 mW of power per trap we reach depths of $U_0/k_B \approx 1$ mK, where k_B is the Boltzmann constant, and radial (longitudinal) trapping frequencies of around 100 kHz (20 kHz). We produce highly uniform microtrap potentials (with peak intensities differing by less than 5% root mean square) via a closed-loop

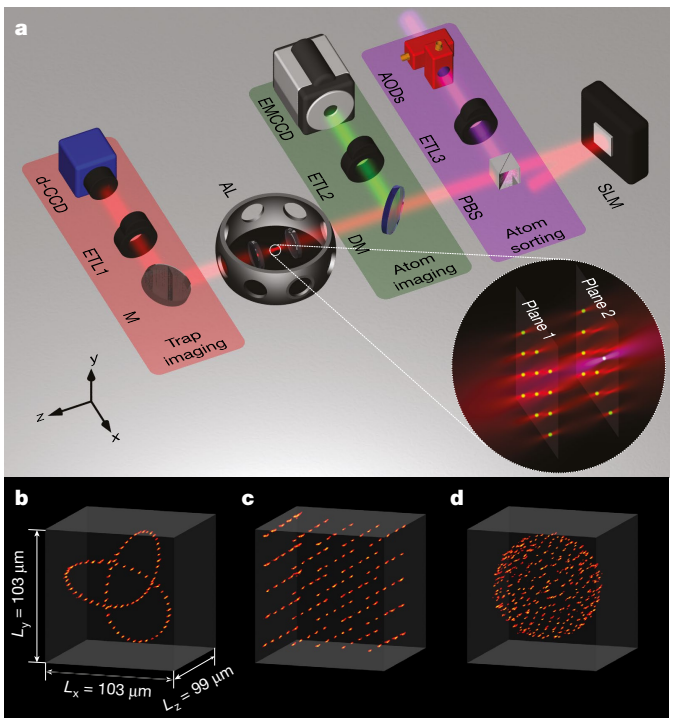

Fig. 1 | Experimental setup and trap images. a, We combine a spatial light modulator (SLM) and a high-numerical-aperture aspheric lens (AL) under vacuum to generate arbitrary 3D arrays of traps. The intensity distribution in the focal plane is measured with the aid of a second aspheric lens, a mirror (M) and a diagnostics CCD camera (d-CCD). The fluorescence of the atoms in the traps at 780 nm is separated from the dipole trap beam with a dichroic mirror (DM) and detected using an electron-multiplying CCD camera (EMCCD). For atom assembly we use moving tweezers superimposed on the trap beam with a polarizing beam splitter (PBS). This extra beam is deflected in the plane perpendicular to the beam propagation with a 2D acousto-optical deflector (AOD), and its focus can be displaced axially by changing the focal length of an electrically tunable lens (ETL3). The remaining electrically tunable lenses (ETL1 and ETL2) in the camera paths allow imaging of different planes along z. The inset depicts the intensity distribution of the trap light forming a bilayer array (red) and the action of the moving tweezers on an individual atom (purple). **b–d**, Intensity reconstructions of exemplary 3D patterns obtained from a collection of z-stack images taken with the diagnostics CCD camera. The regions of maximum intensity form a trefoil knot (**b**), a $5 \times 5 \times 5$ cubic array (**c**) and a C_{320} fullerene-like structure (**d**). The dimensions, L_x, L_y, L_z, of the images are the same in all the examples.

[1]Laboratoire Charles Fabry, Institut d'Optique Graduate School, CNRS, Université Paris-Saclay, Palaiseau, France. [2]These authors contributed equally: Daniel Barredo, Vincent Lienhard, Sylvain de Léséleuc. *e-mail: daniel.barredo@gmail.com

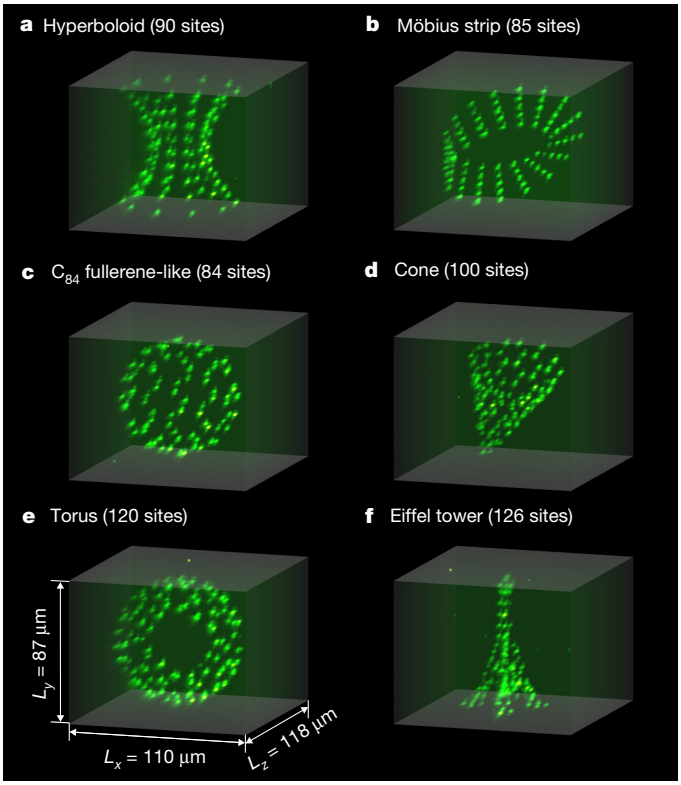

Fig. 2 | Single-atom fluorescence in 3D arrays. a–f, Maximum-intensity-projection reconstruction of the average fluorescence of single atoms loaded stochastically into exemplary arrays of traps. The x, y, z scan range of the fluorescence (L_x, L_y, L_z) is the same for all the 3D reconstructions.

optimization[14]. Rubidium-87 atoms are then loaded in the traps from a magneto-optical trap (MOT), with a final temperature of 25 μK. We detect the occupancy of each trap by collecting the fluorescence of the atoms at 780 nm with an electron-multiplying CCD camera for 50 ms. A second tunable lens (ETL2) in the imaging path is used to focus the fluorescence of different atom planes.

In Fig. 2 we show the fluorescence of single atoms trapped in various complex 3D structures, some of which are relevant, for instance, to the study of non-trivial properties of Chern insulators[19–21]. Each example is reconstructed from a series of 100 z-stack images covering an axial range of about 120 μm. With no further action, these arrays are randomly loaded with a filling fraction of about 0.5; we thus average the fluorescence signal over 300 frames to reveal the geometry of the structures.

For deterministic atom loading, we extend our two-dimensional (2D) atom-by-atom assembler[11] to 3D geometries. For that, we superimpose a second 850-nm laser beam (with $1/e^2$ radius of about 1.3 μm) on the trapping beam, which can be steered in the x–y plane using a 2D acousto-optical deflector and in the z direction by changing the focal length of a third tunable lens (ETL3). Combined with a real-time control system, the moving tweezers can perform single-atom transport with fidelities exceeding 0.993, as shown in ref. [11], and produce fully loaded arrays by using independent and sequential rearrangement of the atoms for each of the n_p planes in the 3D structures.

To explore the feasibility of plane-by-plane atom assembly, we first determine the minimal separation between layers so that each target plane can be reordered without affecting the others. To quantify this, we perform the following experiment in a 2D array containing 46 traps. We randomly load the array with single atoms and demand the atom assembler to remove all the atoms. We average over about 50 realizations and then repeat the experiment for different axial separations between the position of the moving tweezers and the trap plane. The result is shown in Fig. 3a, where we see that for separations beyond about 17 μm the effect of the moving tweezers on the atoms is negligible. This distance can be further reduced to about 14 μm by operating the moving tweezers with less power, without any degradation in the performance of the sorting process. In a complementary experiment, where we fully assembled small arrays, we also checked that the assembling efficiency is not affected by slight changes (below about 3 μm) in the exact axial position of the moving tweezers.

We now demonstrate full loading of arbitrary 3D lattices using plane-by-plane assembly. We start by creating a 3D trap array that can be decomposed in several planes normal to z. In each plane we generate approximately twice the number of traps that we need to load, so that we can easily load enough atoms to assemble the target structure. The sequence used to create fully loaded patterns (see Fig. 3b) starts by loading the MOT and monitoring the atoms entering and leaving the traps by sequentially taking a fluorescence picture for each plane. We trigger the assembler as soon as there are enough atoms in each plane to fully assemble it. We then freeze the loading by dispersing the MOT cloud and record the initial positions of the atoms by another series of z-stack images. Analysis of the images reveals which traps are filled with single atoms. We use this information to compute (in about 1 ms) the moves needed to create the fully loaded target array and perform plane-by-plane assembly by changing the z position of the moving tweezers after the assembly in each plane is completed. Finally, we detect the final 3D configuration with another series of z-stack images.

Figure 3c–h shows a gallery of fully loaded 3D atomic arrays arbitrarily arranged in space. We can create fully loaded 3D architectures with up to 72 atoms distributed in several layers with different degrees of complexity. The selected structures include simple cubic lattices (Fig. 3d), bilayers with square or graphene-like[22] arrangements (Fig. 3c, e, g), lattices with inherent geometrical frustration such as pyrochlore[23] (Fig. 3f) and lattices with cylindrical symmetry (Fig. 3h), which are suitable, for example, for studying quantum Hall physics with neutral atoms[24]. The arrays are not restricted to periodic arrangements, and the positions of the atoms can be controlled with high accuracy (<1 μm). The minimum interlayer separation that we can achieve depends on the type of underlying geometry. This is illustrated in Fig. 3e, which shows the full 3D assembly of a bilayer square lattice (with a layer separation of $d_z = 5$ μm). There, sites corresponding to the second layer are displaced by half the lattice spacing. Because traps belonging to neighbouring layers do not have the same (x, y) coordinates, there is no limitation to the minimum interlayer distance that we can produce. In both images we can observe a defocused fluorescence at intersite positions due to atoms trapped in the neighbouring layer. By contrast, whenever traps are aligned along the z axis (for example, in Fig. 3d), we set a minimum axial separation of about 17 μm to avoid any disturbance from the moving tweezers on the atoms while assembling neighbouring planes. However, for some trapping geometries this constraint can be overcome by applying a small global rotation of the 3D trap pattern around the x or y axis, so that neighbouring traps do not share the same (x, y) coordinates. The minimum interlayer spacing ultimately depends on the Rayleigh range of our trapping beam (about 5 μm) and could be further reduced, for example, by using an aspheric lens with higher numerical aperture. The range of interatomic distances that we can achieve (3– 40 μm) is suitable for implementing fast qubit gates[25] or simulating excitation transport[26] and quantum magnetism with Rydberg atoms, because interaction energies between Rydberg states at those distances are typically in the megahertz range.

To illustrate this possibility, we performed a proof-of-principle experiment with two atoms belonging to the cylindrical lattice displayed in Fig. 3h. The atoms are separated by a total distance of $R_{12} = 20$ μm ($d_x = 10$ μm, $d_z = 17$ μm); see Fig. 4. We first initialize the atoms in state $|g\rangle = |5S_{1/2}, F=2, m_F=2\rangle$, where F and m_F are the hyperfine and magnetic quantum numbers, respectively, by optical pumping in a 47-G magnetic field that defines the quantization axis and is aligned perpendicular to the internuclear axis. Then, the dipole trap is switched off and a two-photon Rydberg stimulated Raman adiabatic passage[27] excites both atoms to the $|\uparrow\rangle = |60S_{1/2}, m_j = 1/2\rangle$ Rydberg state, where m_j is the spin projection along the magnetic field direction.

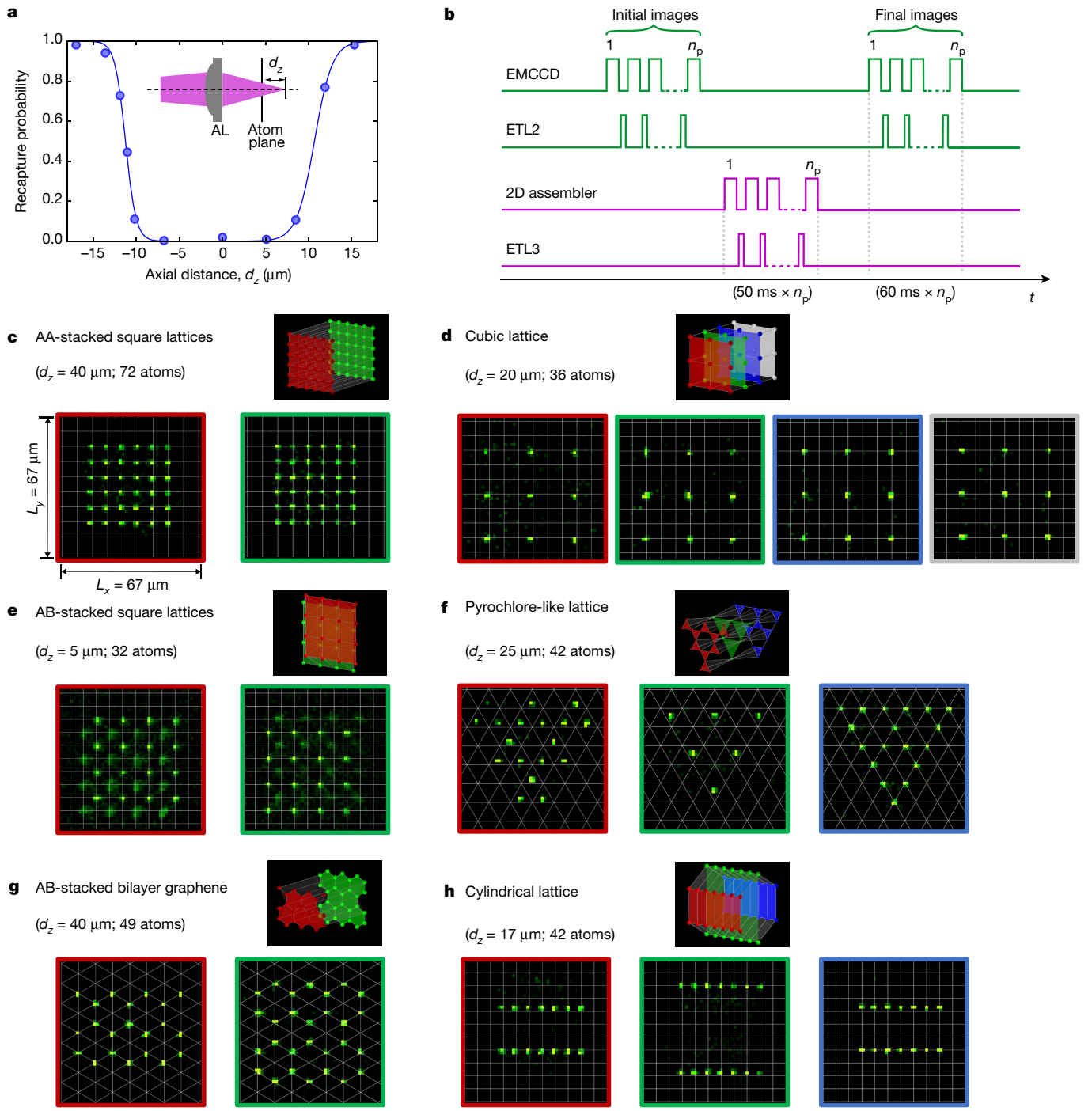

Fig. 3 | Fully loaded 3D arrays of single atoms. a, Recapture probability as a function of the axial distance between the focus of the moving tweezers and the plane of the atoms measured experimentally by trying to remove all the atoms from a 46-trap array. Error bars denote the standard error of the mean and are smaller than the symbol size. The line is a guide to the eye. **b**, Time control sequence of the experiment. We start the experiment by recording sequentially an image for each target plane. The analysis of the resulting n_p images reveals the initial position of the atoms in the traps. The 2D atom assembler, in combination with an electrically tunable lens (ETL3), arranges the atoms plane by plane. Finally, a new set of sequential images is collected to capture the result of the 3D assembly. **c**–**h**, Fully loaded arrays with arbitrary geometries. All images are single shots. The models of the 3D configurations are shown for clarity; the colours of the frames around the images encode successive atomic planes.

We further use a resonant microwave field and local addressing[28] to transfer the second atom to the $|\downarrow\rangle = |60P_{1/2}, m_j = -1/2\rangle$ state, while the first atom remains in $|\uparrow\rangle$. In these two Rydberg levels, the atoms are coupled by a direct dipole–dipole interaction with a strength of $U = C_3/R_{12}^3$, and a calculated C_3 coefficient of $C_3 = h \times 1{,}357\ \mathrm{MHz}\,\mu\mathrm{m}^3$, where h is the Planck constant. The prepared pair-state $|\uparrow\downarrow\rangle$ evolves under the XY-spin Hamiltonian $H = (C_3/R_{12}^3)(\sigma_1^+\sigma_2^- + \sigma_1^-\sigma_2^+)$ (where $\sigma_i^{\pm}$ denotes the Pauli matrices acting on atom $i = \{1, 2\}$) and undergoes coherent spin-exchange oscillations between $|\uparrow\downarrow\rangle$ and $|\downarrow\uparrow\rangle$ as a function of the variable interaction time, T. Finally, a de-excitation sequence projects the population in $|\uparrow\rangle$ to $|g\rangle$, but leaves the population in $|\downarrow\rangle$ unaffected. After switching the dipole trap on again, atoms in $|g\rangle$ are recaptured, while atoms in the excited state $|\downarrow\rangle$ are repelled by the trapping potential of the optical tweezers and appear as atom losses in the final fluorescence images. The outcome of this experiment is shown in Fig. 4. We observe coherent 'flip-flops' between $|\uparrow\downarrow\rangle$ and $|\downarrow\uparrow\rangle$ with a measured frequency of $2U/h = 333 \pm 5$ kHz. This value is consistent with the frequency $2U/h = 339$ kHz expected from our distance

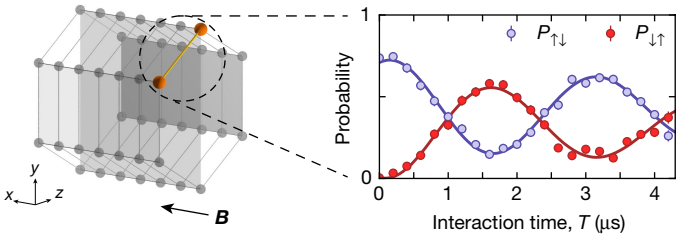

Fig. 4 | Spin-exchange dynamics between two Rydberg atoms in different *z* layers. Excitation-hopping oscillations between $|\uparrow\downarrow\rangle$ and $|\downarrow\uparrow\rangle$, observed in the populations $P_{\uparrow\downarrow}$, $P_{\downarrow\uparrow}$, driven by the dipole–dipole interaction between two Rydberg states, $|\uparrow\rangle = |60S_{1/2}, m_j = 1/2\rangle$ and $|\downarrow\rangle = |60P_{1/2}, m_j = -1/2\rangle$, at a distance of about 20 μm ($d_x = 10\,\mu m$; $d_y = 17\,\mu m$). Error bars represent the standard error of the mean and are mostly smaller than the symbol size. Solid lines are damped sine fits to the data. The direction of the magnetic field, ***B***, is indicated.

calibration ($R_{12} = 20 \pm 1\,\mu m$), which was performed by optical means. The finite contrast and the small damping of the oscillations arise from experimental imperfections (errors in state preparation and readout, residual atomic temperature), as reported in ref. [29]. This proof-of-principle experiment demonstrates the feasibility of performing quantum simulations using our defect-free 3D atomic arrays of single atoms. Excitations hopping under the influence of this Hamiltonian are equivalent to a system of hard-core bosons. The dipole–dipole interactions observed here can be further exploited to engineer Hamiltonians containing complex hopping amplitudes, which are suitable for the study of, for example, topological insulators[30].

Besides the unique tunability of the geometries that it provides, our atom-assembling procedure is highly efficient: we reach typical filling fractions of 0.95. This measured efficiency is slightly dependent on the number of planes and is mainly limited by the lifetime of the atoms in the traps (about 10 s) and the duration of the sequence (we typically need 60 ms per plane to acquire the fluorescence images and about 50 ms per plane to perform atom sorting). The repetition rate of the experiment is about 1 Hz. The number of traps and the filling fraction of the arrays could be further increased with current technology: (i) the volume of the trap array and the maximum number of traps can be extended by increasing the field of view of the aspheric lens and the laser power; (ii) the lifetime of the atoms in the traps can realistically be increased by an order of magnitude; (iii) the repetition rate of the experiment can be increased by optimizing the atom assembler[11], in particular by transferring atoms also between different planes[31]; and (iv) the initial filling fraction of the arrays could reach values exceeding 0.8 by using tailored light-assisted collisions[32,33]. Therefore, the generation of three-dimensional structures containing several hundred atoms at unit filling seems within reach, opening up many new possibilities in quantum information processing and quantum simulation with neutral atoms.

Data availability

The data presented in the figures and that support the other findings of this study are available from the corresponding author on reasonable request.

Online content

Any methods, additional references, Nature Research reporting summaries, source data, statements of data availability and associated accession codes are available at https://doi.org/10.1038/s41586-018-0450-2

Received: 7 December 2017; Accepted: 16 July 2018;
Published online 5 September 2018.

1. Devoret, M. H. & Schoelkopf, R. J. Superconducting circuits for quantum information: an outlook. *Science* **339**, 1169–1174 (2013).
2. Veldhorst, M. et al. A two-qubit logic gate in silicon. *Nature* **526**, 410–414 (2015).
3. Kok, P. et al. Linear optical quantum computing with photonic qubits. *Rev. Mod. Phys.* **79**, 135–174 (2007).
4. Buluta, S. A. I. & Nori, F. Natural and artificial atoms for quantum computation. *Rep. Prog. Phys.* **74**, 104401 (2011).
5. Meschede, D. & Rauschenbeutel, A. Manipulating single atoms. *Adv. At. Mol. Opt. Phys.* **53**, 75–104 (2006).
6. Blatt, R. & Roos, C. F. Quantum simulations with trapped ions. *Nat. Phys.* **8**, 277–284 (2012).
7. Gross, C. & Bloch, I. Quantum simulations with ultracold atoms in optical lattices. *Science* **357**, 995–1001 (2017).
8. Weiss, D. S. & Saffman, M. Quantum computing with neutral atoms. *Phys. Today* **70**, 44–50 (2017).
9. Kuhr, S. Quantum-gas microscopes: a new tool for cold-atom quantum simulators. *Natl Sci. Rev.* **3**, 170–172 (2016).
10. Endres, M. et al. Atom-by-atom assembly of defect-free one-dimensional cold atom arrays. *Science* **354**, 1024–1027 (2016).
11. Barredo, D., de Léséleuc, S., Lienhard, V., Lahaye, T. & Browaeys, A. An atom-by-atom assembler of defect-free arbitrary two-dimensional atomic arrays. *Science* **354**, 1021–1023 (2016).
12. Nelson, K. D., Li, X. & Weiss, D. S. Imaging single atoms in a three-dimensional array. *Nat. Phys.* **3**, 556–560 (2007).
13. Wang, Y., Zhang, X., Corcovilos, T. A., Kumar, A. & Weiss, D. S. Coherent addressing of individual neutral atoms in a 3D optical lattice. *Phys. Rev. Lett.* **115**, 043003 (2015).
14. Nogrette, F. et al. Single-atom trapping in holographic 2D arrays of microtraps with arbitrary geometries. *Phys. Rev. X* **4**, 021034 (2014).
15. Kim, H. et al. In situ single-atom array synthesis using dynamic holographic optical tweezers. *Nat. Commun.* **7**, 13317 (2016).
16. Sturm, M. R., Schlosser, M., Walser, R. & Birkl, G. Quantum simulators by design: many-body physics in reconfigurable arrays of tunnel-coupled traps. *Phys. Rev. A* **95**, 063625 (2017).
17. Di Leonardo, R., Ianni, F. & Ruocco, G. Computer generation of optimal holograms for optical trap arrays. *Opt. Express* **15**, 1913–1922 (2007).
18. Wallis, J. W., Miller, T. R., Lerner, C. A. & Kleerup, E. C. Three-dimensional display in nuclear medicine. *IEEE Trans. Med. Imaging* **8**, 297–303 (1989).
19. Beugeling, W., Quelle, A. & Morais Smith, C. Nontrivial topological states on a Möbius band. *Phys. Rev. B* **89**, 235112 (2014).
20. Rüegg, A., Cof, S. & Moore, J. E. Corner states of topological fullerenes. *Phys. Rev. B* **88**, 155127 (2013).
21. Ningyuan, J., Owens, C., Sommer, A., Schuster, D. & Simon, J. Time- and site-resolved dynamics in a topological circuit. *Phys. Rev. X* **5**, 021031 (2015).
22. Castro Neto, A. H., Guinea, F., Peres, N. M. R., Novoselov, K. S. & Geim, A. K. The electronic properties of graphene. *Rev. Mod. Phys.* **81**, 109–162 (2009).
23. Bramwell, S. T. & Gringas, M. J. P. Spin ice state in frustrated magnetic pyroclore materials. *Science* **294**, 1495–1501 (2001).
24. Łacki, M. et al. Quantum Hall physics with cold atoms in cylindrical optical lattices. *Phys. Rev. A* **93**, 013604 (2016).
25. Saffman, M., Walker, T. G. & Mølmer, K. Quantum information with Rydberg atoms. *Rev. Mod. Phys.* **82**, 2313–2363 (2010).
26. Browaeys, A., Barredo, D. & Lahaye, T. Experimental investigations of dipole–dipole interactions between a few Rydberg atoms. *J. Phys. B* **49**, 152001 (2016).
27. Vitanov, N. V., Rangelov, A. A., Shore, B. W. & Bergmann, K. Stimulated Raman adiabatic passage in physics, chemistry, and beyond. *Rev. Mod. Phys.* **89**, 015006 (2017).
28. de Léséleuc, S., Barredo, D., Lienhard, V., Browaeys, A. & Lahaye, T. Optical control of the resonant dipole–dipole interaction between Rydberg atoms. *Phys. Rev. Lett.* **119**, 053202 (2017).
29. Barredo, D. et al. Coherent excitation transfer in a spin chain of three Rydberg atoms. *Phys. Rev. Lett.* **114**, 113002 (2015).
30. Weber, S. et al. Topologically protected edge states in small Rydberg systems. *Quantum Sci. Technol.* **3**, 044001 (2018).
31. Lee, W., Kim, H. & Ahn, J. Three-dimensional rearrangement of single atoms using actively controlled optical microtraps. *Opt. Express* **24**, 9816–9825 (2016).
32. Grünzweig, T., Hilliard, A., McGoven, M. & Andersen, M. Near-deterministic preparation of a single atom in an optical microtrap. *Nat. Phys.* **6**, 951–954 (2010).
33. Lester, B. J., Luick, N., Kaufman, A. M., Reynolds, C. M. & Regal, C. A. Rapid production of uniformally filled arrays of neutral atoms. *Phys. Rev. Lett.* **115**, 073003 (2015).

Acknowledgements We thank A. Läuchli for discussions. This work benefited from financial support by the EU (H2020 FET-PROACT Project RySQ), by the 'PALM' Labex (projects QUANTICA and XYLOS) and by the Région Île-de-France in the framework of DIM Nano-K.

Reviewer information *Nature* thanks W. Bakr, N. Lundblad and the other anonymous reviewer(s) for their contribution to the peer review of this work.

Author contributions D.B., V.L. and S.d.L. performed the experiments. T.L. and A.B. supervised the work. All authors made critical contributions to the work, discussed the results and contributed to the writing of the manuscript.

Competing interests The authors declare no competing interests.

Additional information
Supplementary information is available for this paper at https://doi.org/10.1038/s41586-018-0450-2.
Reprints and permissions information is available at http://www.nature.com/reprints.
Correspondence and requests for materials should be addressed to D.B.
Publisher's note: Springer Nature remains neutral with regard to jurisdictional claims in published maps and institutional affiliations.